High-grade glioma with pleomorphic and pseudopapillary features (HPAP): a proposed type of circumscribed glioma in adults harboring frequent TP53 mutations and recurrent monosomy 13

HHS Public Access

Author manuscript

Acta Neuropathol. Author manuscript; available in PMC 2023 March 01.

Published in final edited form as:

Acta Neuropathol. 2022 March ; 143(3): 403–414. doi:10.1007/s00401-022-02404-9.

High-grade glioma with pleomorphic and pseudopapillary features (HPAP): a proposed type of circumscribed glioma in adults harboring frequent *TP53* mutations and recurrent monosomy 13

Drew Pratt[1], **Zied Abdullaev**[1], **Antonios Papanicolau-Sengos**[1], **Courtney Ketchum**[1], **Pavalan Panneer Selvam**[1], **Hye-Jung Chung**[1], **Ina Lee**[1], **Mark Raffeld**[1], **Mark R. Gilbert**[2], **Terri S. Armstrong**[2], **Peter Pytel**[3], **Ewa Borys**[4], **Joshua M. Klonoski**[5], **Matthew McCord**[6], **Craig Horbinski**[6], **Daniel Brat**[6], **Arie Perry**[7], **David Solomon**[7], **Charles Eberhart**[8], **Caterina Giannini**[9], **Martha Quezado**[1], **Kenneth Aldape**[1]

[1]Laboratory of Pathology, Center for Cancer Research, National Cancer Institute, Bethesda, MD 20814, USA

[2]Neuro-Oncology Branch, Center for Cancer Research, National Cancer Institute, Bethesda, MD, USA

[3]Department of Pathology, University of Chicago Medicine, Chicago, IL, USA

[4]Department of Pathology, Loyola University Medical Center, Maywood, IL, USA

[5]Department of Pathology and ARUP Laboratories, University of Utah Health Sciences Center, Salt Lake City, USA

[6]Department of Pathology, Feinberg School of Medicine, Northwestern University, Chicago, IL, USA

[7]Department of Pathology, University of California, San Francisco, CA, USA

[8]Department of Neuropathology and Ophthalmic Pathology, Johns Hopkins University, Baltimore, MD, USA

[9]Department of Laboratory Medicine and Pathology, Mayo Clinic, Rochester, MN, USA

Abstract

Tumors of the central nervous system (CNS) often display a wide morphologic spectrum that has, until recently, been the sole basis for tumor classification. The introduction of the integrated histomolecular diagnostic approach in CNS tumors has facilitated a classification system that is increasingly data-driven and with improved alignment to clinical outcome. Here, we report a previously uncharacterized glioma type ($n = 31$) using unsupervised clustering analysis of DNA

Drew Pratt, prattdw@nih.gov; Kenneth Aldape, kenneth.aldape@nih.gov.

Author contributions All authors provided meaningful contributions to the manuscript. All authors read and approved the final manuscript.

Conflict of interest None declared.

Supplementary Information The online version contains supplementary material available at https://doi.org/10.1007/s00401-022-02404-9.

methylation array data from approximately 14,000 CNS tumor samples. Histologic examination revealed circumscribed growth and morphologic similarities to pleomorphic xanthoastrocytoma (PXA), astroblastoma, ependymoma, polymorphous neuroepithelia tumor of the young (PLNTY), and IDH-wildtype glioblastoma (GBM). Median age (46.5 years) was significantly older than other circumscribed gliomas and younger than GBM. Dimensionality reduction with uniform manifold approximation and projection (UMAP) and hierarchical clustering confirmed a methylation signature distinct from known tumor types and methylation classes. DNA sequencing revealed recurrent mutations in *TP53* (57%), *RB1* (26%), *NF1* (26%), and *NF2* (14%) *BRAF* V600E mutations were detected in 3/27 sequenced cases (12%). Copy number analysis showed increased whole chromosome aneuploidy with recurrent loss of chromosome 13 (28/31 cases, 90%). *CDKN2A/B* deletion (2/31, 6%) and *MGMT* promoter methylation (1/31, 3%) were notably rare events. Most tumors showed features of a high-grade glioma, yet survival data showed significantly better overall survival compared to GBM ($p < 0.0001$). In summary, we describe a previously uncharacterized glioma of adults identified by a distinct DNA methylation signature and recurrent loss of chromosome 13.

Introduction

The integration of molecular alterations into the classification of CNS tumors has revealed distinct tumor entities, or types, that often comprise a spectrum of morphologic features. A notable example includes the consolidation of the histologic entities embryonal tumor with abundant neuropil and true rosettes (ETANTR), ependymoblastoma, and medulloepithelioma into a single tumor type called embryonal tumor with multilayered rosettes (ETMR), frequently characterized by alterations in the microRNA cluster C19MC [10] or rarely, by *DICER1* mutations [12, 22]. High-grade astrocytoma with piloid features (HGAP), formerly known as anaplastic astrocytoma with piloid features, is a recently described tumor type that occasionally demonstrates morphologic similarities to glioblastoma (GBM), pilocytic astrocytoma (PA) with anaplastic features, and pleomorphic xanthoastrocytoma (PXA), despite having clinical and molecular features distinct from these tumor types [19]. The characteristic triad of molecular findings in HGAP includes alterations in the MAPK pathway (*NF1* mutation/deletion in 30%, *BRAF* fusions in 20%, *FGFR1* mutation/fusion in 19%, *KRAS* in 3%, and *BRAF* V600E mutation in 1% of cases), *CDKN2A/B* deletion or mutation (80% of cases), and alterations in telomere maintenance (*ATRX* mutation in 45% and *TERT* promoter mutation in 3% of cases) [19]. Importantly, the identification of alterations in these three pathways is neither necessary nor sufficient for the diagnosis of HGAP. In fact, 25% of cases in the study by Reinhardt et al. lacked a detectable MAPK alteration, while two cases did not harbor alterations in any of these pathways. Despite this complex genetic profile, HGAP is identified by a distinct epigenetic signature with DNA methylation array profiling [3, 5, 6, 19], and methylation is the sole molecular diagnostic criterion for this tumor type in the 2021 WHO Classification of Central Nervous System Tumors [12].

Histologically, gliomas have traditionally been separated into two major groups based on infiltrating (“diffuse”) and non-infiltrating (“circumscribed”) growth patterns. Circumscribed gliomas often occur in younger individuals and include tumor types such as PA,

PXA, subependymal giant cell astrocytoma (SEGA), chordoid glioma, ependymoma, subependymoma, and astroblastoma. While the molecular features of these tumors have been increasingly elucidated in recent years, there remains a subset of cases that do not demonstrate the characteristic clinical and/or molecular features for these tumor types. For example, astroblastoma, a glial neoplasm with distinctive perivascular pseudorosettes, is now defined by an *MN1* (22q12.1) gene fusion involving *BEND2* (Xp22.13) or rarely *CXXC5* (5q31.2) [21]. Rare examples feature *BEND2* fusion with other partners, such as *EWSR1* (22q12) [25]. A recent molecular analysis of histologically defined astroblastomas revealed that a subset of these tumors resolve into other established CNS WHO diagnoses such as PXA and *ZFTA* (formerly *RELA*) fusion-positive supratentorial ependymoma [11]. Furthermore, a small subset of these tumors failed to resolve into a known tumor type entirely. A separate study similarly reclassified a subset of histologically defined astroblastomas into PXA and GBM based on sequencing and methylation profiling [4]. Thus, there is significant clinicopathologic heterogeneity in *MN1*-intact gliomas with astroblastoma-like histologic features, some of which harbor molecular features of PXA (e.g., *BRAF* V600E mutation, DNA methylation profile) and display high-grade features reminiscent of GBM.

Herein, we describe the clinical, histologic, and molecular features of a group of circumscribed, predominantly high-grade gliomas primarily occurring in young adults that is associated with a relatively favorable clinical outcome. While these tumors often showed histologic similarities to both high-grade (GBM, anaplastic PXA, anaplastic ependymoma) and low-grade (astroblastoma, PLNTY) gliomas or glioneuronal tumors, we show that the diverse histology and mutational profile of this group resolves into a single nosologic type based on DNA methylation and the presence of chromosome 13 loss in almost all cases, clearly distinguishing them from other circumscribed and diffuse gliomas.

Materials and methods

Samples and datasets

This study included previously published cases for which the raw methylation array data (IDAT format, 450 K/EPIC platform) was available and cases profiled through the consult service at the National Institutes of Health/National Cancer Institute (NIH/NCI) Laboratory of Pathology in Bethesda, Maryland. Publicly available methylation data were acquired from the following sources: PMID: 28966033 (E-MTAB-5528), PMID: 30876455 (GSE125450), PMID: 31346129 (E-MTAB-7490), and PMID: 32991787 (GSE143843). The remaining samples were procured from in-house cases and the following collaborating institutions: Johns Hopkins Medical Institute (Baltimore, Maryland); Mayo Clinic (Rochester, Minnesota); University of California San Francisco Medical Center (San Francisco, California); University of Chicago (Chicago, Illinois); Loyola University Medical Center (Maywood, Illinois); and the University of Utah (Salt Lake City, Utah). Sample collection and processing and data collection were performed in accordance with local ethics regulations and approval.

Histology and immunohistochemistry

Representative 5-μm-thick sections from formalin-fixed paraffin embedded (FFPE) blocks were used for histochemical and immunohistochemical studies. Where available, immunohistochemical staining of cases at the NIH/NCI for glial fibrillary acidic protein (GFAP), epithelial membrane antigen (EMA), Ki-67, CD34, and OLIG2 was performed using automated immunohistochemistry Roche-Ventana Bench-Mark Ultra (Roche Diagnostics Corporation, Indianapolis, USA). Stained slides were scanned with the NanoZoomer S210 Digital Slide Scanner (Hamamatsu, Japan).

DNA methylation profiling

Samples with tumor cellularity over 60%, wherever possible, were selected for DNA methylation profiling, which was performed as previously described [24]. Genomic DNA (target amount > 250 ng) was bisulfite-converted (EZ DNA Methylation Kit, Zymo Research D5001). Bisulfite-converted FFPE DNA was processed with the Infinium FFPE DNA Restore kit (Illumina, USA) and was assayed on the Infinium MethylationEPIC kit (Illumina, USA), according to the Infinium HD FFPE Methylation Assay automated protocol (Illumina, USA).

Bioinformatic analyses

For unsupervised clustering of samples, IDAT files from both platforms (450 K, EPIC) were first normalized using the functional normalization procedure from the Meffil R package [15] as follows: background correction and dye bias correction was performed using a 450 K/EPIC common feature set. Methylated and unmethylated signals were then compared and outlier samples whose predicted median methylated signal was more than three standard deviations from the expected were removed. Samples with the following probe quality control results were removed: control probe deviations from the mean, proportion of > 0.2 of probes with a detection p value > 0.01, proportion of probes > 0.2 with a bead number < 3, and proportion of samples with a detection p value > 0.01 is > 0.2 (i.e., only background signal in a high proportion of probes). Next, the number of principal components of the control matrix was determined to include in quantile normalization. This was done through visual assessment of plotting the quantile residuals after fitting different numbers of control matrix PCs. Control probe variance was then removed from the sample quantiles with the array type (450 K, EPIC) included as a fixed effects variable. Samples were then normalized using their normalized quality control objects with the aforementioned CpGs removed. The following probes were then removed from the combined normalized signals: probes mapping to X or Y chromosomes, probes where the 30 bp 3′-subsequence is non-unique, probes masked for mapping reasons, probes masked for extension base inconsistent with specified color channel (type I) or CpG (type II) based on mapping, probe has a SNP in the extension base that causes a color channel switch from the official annotation, and probes where the 5 bp 3′-subsequence (including extension for type II) overlap with any of the SNPs with global MAF > 1% (http://zwdzwd.github.io/InfiniumAnnotation) [26]

For clustering and dimensionality reduction, feature selection was performed by reducing the beta value matrix to the most variable probes by standard deviation (> 0.27 and > 0.21 for the pan-CNS and focused unsupervised embeddings, respectively). The number

of principal components (PC) used for dimensionality reduction were 150 and 40 for the pan-CNS and focused unsupervised embeddings, respectively. Dimensionality reduction on the PC matrix was then performed using the uniform manifold approximation and projection (UMAP) method (uwot R package) with the following non-default parameters: n_neighbors = 10, spread = 2, min_dist = 0.2. Visualization using t-distributed stochastic neighbor embedding (t-SNE) was performed using the Rtsne package with the following parameters: perplexity = 10, iterations = 2500, theta = 0. Tumor samples were separately classified using v11 [5] of the CNS tumor methylation classifier (https://www.molecularneuropathology.org/mnp). We used a classification calibrated score cut-off > 0.9 denoting a high confidence classification, unless otherwise specified. Agglomerative hierarchical clustering was performed on the reduced beta value matrix using the Euclidean distance metric and ward.D2 linkage method.

Genome-wide copy number estimation

Copy number profiling was performed on raw methylation signal intensities using the Conumee R package with an additional baseline correction, as previously described [9]. A non-default parameter of minimum width = 3 was used. Regions excluded from analysis included: probes where the 30 bp 3′-subsequence is non-unique, and probes where the 5 bp 3′-subsequence (including extension for type II) overlap with any of the SNPs with global MAF > 1%. Copy number data from male and female samples were generated separately. Focal copy number alterations (i.e., deletions, amplifications) were called based on manual review of the $\log_2$ ratio plots for each sample. Broad copy number calls (i.e., gain, loss) were made based on a threshold of 0.1 $\log_2$ ratio.

MGMT promoter methylation estimation

MGMT promoter methylation status was derived from DNA methylation array data using a previously published method [1, 2].

Targeted next generation sequencing

For cases sequenced at the NIH/NCI (TSO500, PBTP), Genomic DNA and RNA was extracted from 5 μm sections of formalin-fixed paraffin embedded tissue (FFPE) sections using the AllPrep DNA/RNA FFPE Kit (Qiagen, Hilden, Germany). A portion of the DNA was set aside for methylation analysis as previously described. Next generation sequencing (NGS) was performed using either a custom amplicon-based brain tumor specific panel (PBTP) [18], or a commercial panel TruSight Oncology 500 (TSO 500; Illumina, San Diego, USA). The TSO500 panel contents can be found on the manufacturer's website: https://www.illumina.com/products/by-type/clinical-research-products/trusight-oncology-500.html). For the Ion Torrent based panel (PBTP), libraries were generated from genomic DNA and cDNA using AmpliSeq technology and subjected to next generation sequencing using Ion S5™ XL Sequencing System (Thermo Fisher Scientific). Signal processing, base calling, and alignment to the GRCh37/hg19 human genome assembly were carried out using Torrent Suite™ software packages (Thermo Fisher Scientific). Variant annotation and interpretation were performed with Ion Reporter Software v.5.10 (Thermo Fisher Scientific). Illumina platform libraries were prepared using TruSight Oncology 500 kit according to the manufacturer's instructions. Amplified pre-enriched

libraries were hybridized to probes specific to the 523 genes targeted by the TruSight Oncology 500 panel. Enriched libraries were amplified, quantified, and normalized to 2 nM, then sequenced as paired-end reads on a high-output NextSeq 500/550 flow cell. TruSight Oncology 500 local app was used for alignment, variant calling, and determination of TMB and MSI. All variants were manually reviewed by visualizing the raw sequencing read alignments using the Integrative Genomics Viewer [20]. Final interpretation of variants was based on an integration of data from multiple bioinformatics databases and experimental and clinical data reported in the biomedical literature. For a subset of cases, sequencing was performed from outside institutions and results reported as part of the consultation process. The specific panels are list in Supplementary table (online resource).

Statistical analysis

For comparison of copy number proportions, a two-sided Fisher's exact test was used with correction for multiple testing (Benjamini–Hochberg method). A two-tailed Student's t test was used for comparison of age. Survival curves were estimated using the Kaplan–Meier method and differences were tested with the log-rank test. A p value < 0.05 was considered statistically significant, unless otherwise specified.

Results

DNA methylation profiling reveals a previously undescribed group of tumors near the PXA and PLNTY clusters

Through unsupervised clustering of DNA methylation profiles from approximately 14,000 CNS samples, we identified a group of tumors ($n = 31$) in close proximity to, but distinct from, PXA and PLNTY that did not match to a known methylation class (score < 0.9) with v11 of the Heidelberg Classifier [5] (https://www.molecularneuropathology.org/mnp; Supplementary Fig. 1a, online resource). This group was comprised of tumors with a variety of diagnoses including anaplastic PXA, astroblastoma, anaplastic ependymoma, PLNTY, and glioblastoma (Supplementary table, online resource; also see detailed description of the morphologic features below). Unsupervised embedding (UMAP, t-SNE), along with representative samples among tumor types with similar histologic and molecular features (see genetic info below), confirmed these tumors as a distinct group (Fig. 1a; Supplementary Fig. 1b, online resource). The clustering of these tumors in the low-dimensional space was confirmed with hierarchical clustering among PXA, PLNTY, and *MN1*-altered astroblastomas, tumor types with striking morphologic similarities to this group (Fig. 1b). Clustering also identified two potential subtypes, A and B, which was largely confirmed with both methodologies. As shown in Fig. 1b, this previously undescribed group shows epigenetic similarities to PXA and PLNTY across standard functional regions of the genome (regions in relation to gene promoters and CpG islands). Using the predominant morphologic features observed in these samples (described below), we propose the descriptive but representative name *High-grade glioma with pleomorphic and pseudopapillary features* (HPAP).

HPAPs are enriched for TP53, RB1, and NF1 mutations with recurrent monosomy 13 and relative absence of CDKN2A/B homozygous deletions

Targeted next generation sequencing (NGS) (see Methods) identified inactivating alterations in *TP53* (13/23 profiled samples, 57%), *RB1* (6/23, 26%), *NF1* (6/23, 26%), and *NF2* (3/21, 14%) (Fig. 2a; Supplementary table, online resource). Three cases (12%) harbored a *BRAF* V600E activating mutation, which was mutually exclusive with inactivating mutations in the aforementioned tumor suppressor genes (TSG). This genetic profile was also clearly distinct from the morphologically similar PXA (Fig. 2a). There was no apparent enrichment in the distribution of the TSG mutations (*TP53, RB1, NF1*) among the functional domains for these genes (Supplementary Fig. 2a-c, online resource). There was a slight difference in the frequency of *TERT* promoter mutations between HPAP and PXA (8% vs. 21% among HPAP and PXA, respectively).

Copy number profiles derived from methylation array data showed whole chromosome aneuploidy with frequent losses involving chromosomes 3, 6, 10–15, 17, 18, and 22, and gains involving chromosomes 4q, 5, 7, and 19 (Fig. 2b). Nearly all cases (28/31) harbored loss of the entirety of chromosome 13. When compared with PXA, the frequency of whole chromosome loss was significantly enriched among HPAPs for chromosomes 3, 11–14, 15, 17, 18, and 22 (Fig. 2c). Conversely, the only significantly enriched region identified in PXA was the 9p21 locus involving the *CDKN2A/B* genes (adjusted $p < 0.0001$, two-sided Fisher's exact test; Fig. 2c). Interestingly, all three HPAP cases that harbored a *BRAF* V600E mutation did *not* show concurrent *CDKN2A/B* homozygous deletion. Similar differences were observed when compared with PLNTY and showed significant losses in chromosomes 3, 6, 11–15, 17, and 18 (Fig. 2c). When comparing the CNV profile of HPAP to GBM, there were four cases (Cases 2, 9, 30, and 31; 4/31, 13%) demonstrating the + 7/− 10 copy number pattern common to adult-type GBM (Supplementary Fig. 3a, online resource). Case 9 was from a 57-year-old man initially diagnosed as an IDH-wildtype GBM harboring *RB1* and *TP53* mutations and negative for *TERT* promoter mutation. Histology revealed a circumscribed growth pattern with increased mitotic activity, microvascular proliferation, and necrosis. The tumor recurred after 59 months and the patient was alive at last follow-up, 74 months (6.2 years) after diagnosis, indicative of a survival time that would be unexpected for GBM. Case 2 was previously published as part of a pediatric high-grade glioma series (pHGG_META_0193) [14] and occurred in a 24-year-old woman with a reported histologic diagnosis of anaplastic ganglioglioma; the patient was reported to be alive 24 months after diagnosis. Genome-wide copy number plots for all samples included in this study can be found in the Supplementary material (online resource).

Analysis of HPAP subtypes revealed enrichment of specific somatic alterations. *BRAF* V600E mutations were exclusively observed in subtype B (3/13 cases), but not all subtype B tumors harbored this mutation (Fig. 2a). Chromosome 7 gain was more frequent in subtype B (10/16 cases versus 3/15 in subtype A), while subtype A showed numerous whole chromosome losses involving 3, 11–15, 17, 18, and 22 (Supplementary Fig. 3b, online resource). Both subtypes showed near-universal loss of chromosome 13.

Interrogation for potential fusions was performed in 21/31 cases using both whole-transcriptome RNA-seq (4/21) and targeted sequencing (20/21) (see Methods). Case 3

harbored a *KCTD8-NTRK2* fusion, but recurrent fusions, including those involving *MN1* or *EWSR1* [13], were not identified in the samples evaluated. *MGMT* promoter methylation (calculated from methylation array data) was present in only 1/31 cases (0.3%).

Histologic features resemble multiple tumor types including anaplastic PXA, astroblastoma, anaplastic ependymoma, PLNTY, and glioblastoma

The majority of cases in this group had been given a histologic diagnosis or impression of glioblastoma (9/30), anaplastic pleomorphic xanthoastrocytoma (3/30), astroblastoma with and without anaplasia (7/30), or anaplastic ependymoma (5/30). A minority of cases demonstrated lower grade histology and were identified as pilocytic astrocytoma (1/30), PLNTY/ganglioglioma (2/30), or simply ‘low-grade glial or glioneuronal tumor’ (1/30) and ‘glioma’ (3/30). Indeed, review of H&E-stained slides from a large subset (23/31) showed a wide range of morphologic and architectural features. A recognizable feature, when present, was marked pleomorphism of tumor nuclei, often with giant cell morphology and multinucleation (Fig. 3a, b). In contrast, some tumors showed monomorphic nuclear features (Fig. 3c). Eosinophilic granular bodies were occasionally identified. A distinctive feature overlapping with PLNTY was the focal presence of oligodendroglial-like perinuclear clearing in pleomorphic tumor cells, but this was only seen in a minority of cases (Fig. 3d, e). One tumor demonstrated an ependymoma-like appearance with elongated cells in perivascular arrangements including nuclear-free fibrillary zones (Fig. 3f). Loss of cellular cohesion, leading to pseudopapillary structures was another frequent and distinctive finding, but these were not present in every case (Fig. 3g-i). One tumor displayed a prominent mucinous matrix admixed with more typical perivascular pseudorosettes (Fig. 3j). Finally, all tumors for which histologic information and/or H&E-stained slides were available showed a predominantly non-infiltrative appearance, with tumors often appearing well-delineated from the adjacent non-neoplastic brain tissue (Fig. 3k,l).

Features typically associated with higher grade (mitotic figures, elevated Ki-67 labeling index, microvascular proliferation, necrosis) were observed or reported in most cases (Fig. 4a; Supplementary Fig. 4, online resource; Supplementary table, online resource). Mitotic activity ranged from inconspicuous to > 10 per 10 hpf with atypical forms present in some cases (Supplementary Fig. 4a, online resource). Necrosis and microvascular proliferation were present in approximately half of the cases (Supplementary Fig. 4b, online resource). Immunohistochemistry was performed and/or reported in most cases. In cases that were stained with GFAP (22/31), all were either diffusely positive (19/22) or showed patchy immunoreactivity (3/22) (Fig. 4a). OLIG2, CD34, and EMA were inconsistently expressed (Supplementary Fig. 5a-c, online resource). Staining for OLIG2 ranged from negative to diffusely positive in tumor nuclei (Supplementary Fig. 5d-f, online resource). CD34 staining showed a range of membranous and cytoplasmic expression patterns, with occasional cases being completely negative (Supplementary Fig. 5 g-i, online resource); these features could be seen within regions of the same tumor. Increased reticulin deposition, a feature often observed in PXA, was not identified in 4/4 cases.

It should be noted that none of these histologic features were present in all cases (low sensitivity) and most are seen in other established CNS WHO tumor types (low specificity).

Additionally, multiple patterns and cellular morphologies could be observed within a single case. There was no observed association of morphology and/or immunophenotype with specific subtypes or genetic alterations (Supplementary Fig. 6, online resource), suggesting that histologic criteria alone will likely be insufficient to identify this tumor type. Digital images from scanned slides have been made available from representative cases (see Data availability).

Clinical characteristics and outcome

The mean and median age at diagnosis for HPAP was 46.4 and 46.5 years (range 14–71), respectively. This was significantly older than PXA (mean/median of 21.3 and 18.5 years; $p < 0.0001$), pilocytic astrocytoma, posterior fossa (PA_PF) (17.5/20; $p < 0.0001$), pilocytic astrocytoma, midline (PA_MID) (6/4; $p < 0.0001$), astroblastoma, MN1-altered (AB_MN1) (15.9/14; $p < 0.0001$), and PLNTY (17.3/12; $p < 0.0001$), as well as being significantly younger than glioblastoma with primitive neuroectodermal features (GBM_PNET) (59.5/62; $p < 0.01$) and IDH-wildtype glioblastoma (MCF_GBM) (56.5/57; $p < 0.01$) (Fig. 4b; see figure caption for description of methylation class abbreviations). Additionally, subtype analysis showed cases in subtype A (mean age 51 years) were significantly older than those in subtype B (mean age 41.8 years, $p < 0.05$; Fig. 4c). There was a slight female predominance present in all cases as well as among subtypes (Fig. 4d). Tumors occurred across both the supratentorial and infratentorial compartments and had no predilection for a specific neuroanatomic site (Fig. 4e), although most occurred in the frontal lobes. There were no cases found to occur in the spinal cord in the current study.

Details regarding initial radiography were limited, but reports containing descriptions or excerpts of imaging features were available for twelve cases (Supplementary table, online resource). Three cases described features of a non-infiltrating neoplasm (e.g., “circumscribed”, “expansile”); among these, an “extra-axial” mass was described in two cases. Enhancement patterns were described as heterogeneous, nodular, and solid. A cystic component was mentioned in six cases and calcifications were noted in two cases.

Clinical outcome (overall survival, OS) data were available for 20/31 samples (11 females, 9 males). The median follow-up time was 42.5 months (Fig. 4f). Cases clustering with HPAP showed significantly better OS than IDH-wildtype GBM (MCF_GBM, $p \leq 0.0001$, Fig. 4f); this survival difference remained significant even after filtering for histologic features diagnostic of GBM in HPAP (i.e., microvascular proliferation and/or necrosis; $p \leq 0.0001$, Supplementary Fig. 7a, online resource). When compared to samples in the PXA and HGAP methylation classes, HPAP showed no significant difference in OS ($p = 0.096$ and $p = 0.056$, respectively; Fig. 4f). Most cases in our study within the PXA group, for which survival data were available, contained high-grade histology (i.e., WHO grade 3) and when filtering PXA and HPAP samples meeting diagnostic criteria for anaplastic PXA (≥ 5 mitoses per 10 hpf), there remained no significant difference in OS ($p = 0.64$, Supplementary Fig. 7b, online resource). There was also no significant difference in OS between HPAP and pilocytic astrocytoma (MCF_PA; $p = 0.47$), *MN1*-altered astroblastoma ($p = 0.29$), and PLNTY ($p = 0.2$; Fig. 4f).

HPAP demonstrates global hypermethylation with differential CpG island and enhancer methylation

We performed additional analyses to characterize aberrant methylation patterns seen in this newly identified group. For downstream analyses, we chose PXA and PLNTY as comparator groups due to the morphologic and epigenetic similarity observed in HPAP (e.g., frequent nuclear pleomorphism, circumscription, and proximity to PXA and PLNTY in the low-dimensional space among CNS tumors). Differential methylation between these groups showed an overall increase in hypermethylation of interrogated CpG sites (Fig. 5a). Further analysis of these differentially methylated regions showed inverse enrichment of CpG islands (CGI) and open sea probes (interCGI) among the tumor types examined: compared to PXA, HPAP showed greater hypermethylation of interCGI and hypomethylation of CGI (Fig. 5b). Conversely, CGI were found to be significantly hypermethylated in HPAP compared to PLNTY. Analysis of gene regulatory regions similarly showed inverse patterns of differential methylation: when compared with PXA, tumors showed increased hypermethylation of enhancer regions, while a comparison with PLNTY revealed hypomethylation of gene enhancers (Fig. 5c).

Discussion

Here, we describe a previously uncharacterized group of predominantly high-grade circumscribed gliomas occurring in young adults. These tumors, which we have preliminarily termed *high-grade glioma with pleomorphic and pseudopapillary features* (HPAP), often demonstrate histologic features that overlap with previously established CNS tumor types including PXA, ependymoma, astroblastoma, PLNTY, and glioblastoma. DNA methylation profiling reveals a common DNA methylation signature that defines this group and shows clustering that is distinct from other CNS tumor types. DNA sequencing revealed recurrent deleterious alterations in *TP53, NF1, NF2, RB1*, and *BRAF*. A near-universal finding was the presence of chromosome 13 loss, in addition to frequent whole chromosome aneuploidy. Patient outcome data showed that even among tumors with GBM-like histology, survival was favorable compared to GBM. Taken together, these findings warrant consideration of this group of tumors as distinct from current recognized CNS tumor types. Given the wide spectrum of histologic features, key diagnostic criteria would necessitate additional molecular testing, and may include features such as a non-infiltrative glioma with multiple whole chromosome copy number changes (loss of chromosome 13 and lack of CDKN2A/B deletion are highly congruent with the diagnosis), and an appropriate mutational profile in conjunction with a ‘no match’ DNA methylation profile result using the with the machine learning-based (Heidelberg) classifier (v11b4).

In gliomas, success with targeted therapeutics has largely been demonstrated in tumors with identifiable driver alterations [7]. Interim results were recently published from the ROAR (Rare Oncology Agnostic Research) trial investigating *BRAF/MEK* combination targeted therapy in *BRAF*-mutant cancers [23]. The results showed a durable radiographic response in *BRAF*-mutant high- (33%) and low-grade (69%) gliomas based on RANO (Response Assessment in Neuro-Oncology) criteria [17, 23]. Interestingly, a separate study identified an additional dependency in MAPK driven tumors through *DUSP4/6* deletion as a synthetic

lethal target in *BRAF*-mutant melanomas and may provide a mechanism for averting MAPK inhibitor resistance8. Perturbations in the RB1 pathway, and the consequent cell cycle deregulation, may also represent a therapeutic vulnerability for RB1-deficient tumors with *CDK4/6* inhibition [16]. Therefore, the constellation of genetic alterations detected in this proposed group may warrant certain considerations for targeted therapy.

Conclusion

In summary, we describe the identification of a new epigenetically defined group of high-grade circumscribed gliomas that are primarily found in young adults and harbor chromosome 13 loss and mutations in *RB1, NF1, NF2, BRAF* V600E, and *TP53*. We propose the name *high-grade glioma with pleomorphic and pseudopapillary features* (HPAP) to reflect the predominant and recognizable histologic features. Importantly, a substantial proportion of these tumors demonstrated features of glioblastoma yet showed a significantly better clinical outcome.

Supplementary Material

Refer to Web version on PubMed Central for supplementary material.

Acknowledgements

The authors gratefully acknowledge all patients and their families. This work utilized the computational resources of the NIH HPC Biowulf cluster (https://hpc.nih.gov/systems/).

Data availability

Whole-slide images of H&E-stained slides from select cases are available for viewing at: https://figshare.com/projects/High-grade_glioma_with_pleomorphic_and_pseudopapillary_features/127778. The raw methylation array data (IDAT format) has been made available for download at the Gene Expression Omnibus (GEO) repository under the accession number GSE195567 (https://www.ncbi.nlm.nih.gov/geo/).

References

1. Bady P, Delorenzi M, Hegi ME (2016) Sensitivity ANALYSIS OF THE MGMT-STP27 model and impact of genetic and epigenetic context to predict the mgmt methylation status in gliomas and other tumors. J Mol Diagn 18:350–361. 10.1016/j.jmoldx.2015.11.009 [PubMed: 26927331]
2. Bady P, Sciuscio D, Diserens AC, Bloch J, van den Bent MJ, Marosi C et al. (2012) MGMT methylation analysis of glioblastoma on the Infinium methylation BeadChip identifies two distinct CpG regions associated with gene silencing and outcome, yielding a prediction model for comparisons across datasets, tumor grades, and CIMP-status. Acta Neuropathol 124:547–560. 10.1007/s00401-012-1016-2 [PubMed: 22810491]
3. Bender K, Perez E, Chirica M, Onken J, Kahn J, Brenner W et al. (2021) High-grade astrocytoma with piloid features (HGAP): the Charite experience with a new central nervous system tumor entity. J Neurooncol 153:109–120. 10.1007/s11060-021-03749-z [PubMed: 33905054]
4. Boisseau W, Euskirchen P, Mokhtari K, Dehais C, Touat M, Hoang-Xuan K et al. (2019) Molecular profiling reclassifies adult astroblastoma into known and clinically distinct tumor entities with

frequent mitogen-activated protein kinase pathway alterations. Oncologist 24:1584–1592. 10.1634/theoncologist.2019-0223 [PubMed: 31346129]

5. Capper D, Jones DTW, Sill M, Hovestadt V, Schrimpf D, Sturm D et al. (2018) DNA methylation-based classification of central nervous system tumours. Nature 555:469–474. 10.1038/nature26000 [PubMed: 29539639]
6. Capper D, Stichel D, Sahm F, Jones DTW, Schrimpf D, Sill M et al. (2018) Practical implementation of DNA methylation and copy-number-based CNS tumor diagnostics: the Heidelberg experience. Acta Neuropathol 136:181–210. 10.1007/s00401-018-1879-y [PubMed: 29967940]
7. Ghiaseddin A, Hoang Minh LB, Janiszewska M, Shin D, Wick W, Mitchell DA et al. (2021) Adult precision medicine: learning from the past to enhance the future. Neurooncol Adv 3:145. 10.1093/noajnl/vdaa145
8. Ito T, Young MJ, Li R, Jain S, Wernitznig A, Krill-Burger JM et al. (2021) Paralog knockout profiling identifies DUSP4 and DUSP6 as a digenic dependence in MAPK pathway-driven cancers. Nat Genet. 10.1038/s41588-021-00967-z
9. Koelsche C, Schrimpf D, Stichel D, Sill M, Sahm F, Reuss DE et al. (2021) Sarcoma classification by DNA methylation profiling. Nat Commun 12:498. 10.1038/s41467-020-20603-4 [PubMed: 33479225]
10. Korshunov A, Sturm D, Ryzhova M, Hovestadt V, Gessi M, Jones DT et al. (2014) Embryonal tumor with abundant neuropil and true rosettes (ETANTR), ependymoblastoma, and medulloepithelioma share molecular similarity and comprise a single clinicopathological entity. Acta Neuropathol 128:279–289. 10.1007/s00401-013-1228-0 [PubMed: 24337497]
11. Lehman NL, Usubalieva A, Lin T, Allen SJ, Tran QT, Mobley BC et al. (2019) Genomic analysis demonstrates that histologically-defined astroblastomas are molecularly heterogeneous and that tumors with MN1 rearrangement exhibit the most favorable prognosis. Acta Neuropathol Commun 7:42. 10.1186/s40478-019-0689-3 [PubMed: 30876455]
12. Louis DN, Perry A, Wesseling P, Brat DJ, Cree IA, Figarella-Branger D et al. (2021) The 2021 WHO classification of tumors of the central nervous system: a summary. Neuro Oncol 23:1231–1251. 10.1093/neuonc/noab106 [PubMed: 34185076]
13. Lucas CG, Gupta R, Wu J, Shah K, Ravindranathan A, Barreto J et al. (2021) EWSR1-BEND2 fusion defines an epigenetically distinct subtype of astroblastoma. Acta Neuropathol. 10.1007/s00401-021-02388-y
14. Mackay A, Burford A, Carvalho D, Izquierdo E, Fazal-Salom J, Taylor KR et al. (2017) Integrated molecular meta-analysis of 1000 pediatric high-grade and diffuse intrinsic pontine glioma. Cancer Cell 32(520–537):e525. 10.1016/j.ccell.2017.08.017
15. Min JL, Hemani G, Davey Smith G, Relton C, Suderman M (2018) Meffil: efficient normalization and analysis of very large DNA methylation datasets. Bioinformatics 34:3983–3989. 10.1093/bioinformatics/bty476 [PubMed: 29931280]
16. O'Leary B, Finn RS, Turner NC (2016) Treating cancer with selective CDK4/6 inhibitors. Nat Rev Clin Oncol 13:417–430. 10.1038/nrclinonc.2016.26 [PubMed: 27030077]
17. Peters KB (2021) Targeting BRAF-mutant glioma: reflections on the ROAR trial. Lancet Oncol. 10.1016/S1470-2045(21)00662-8
18. Raffeld M, Abdullaev Z, Pack SD, Xi L, Nagaraj S, Briceno N et al. (2020) High level MYCN amplification and distinct methylation signature define an aggressive subtype of spinal cord ependymoma. Acta Neuropathol Commun 8:101. 10.1186/s40478-020-00973-y [PubMed: 32641156]
19. Reinhardt A, Stichel D, Schrimpf D, Sahm F, Korshunov A, Reuss DE et al. (2018) Anaplastic astrocytoma with piloid features, a novel molecular class of IDH wildtype glioma with recurrent MAPK pathway, CDKN2A/B and ATRX alterations. Acta Neuropathol 136:273–291. 10.1007/s00401-018-1837-8 [PubMed: 29564591]
20. Robinson JT, Thorvaldsdottir H, Winckler W, Guttman M, Lander ES, Getz G et al. (2011) Integrative genomics viewer. Nat Biotechnol 29:24–26. 10.1038/nbt.1754 [PubMed: 21221095]

21. Sturm D, Orr BA, Toprak UH, Hovestadt V, Jones DTW, Capper D et al. (2016) New brain tumor entities emerge from molecular classification of CNS-PNETs. Cell 164:1060–1072. 10.1016/j.cell.2016.01.015 [PubMed: 26919435]

22. Uro-Coste E, Masliah-Planchon J, Siegfried A, Blanluet M, Lambo S, Kool M et al. (2019) ETMR-like infantile cerebellar embryonal tumors in the extended morphologic spectrum of DICER1-related tumors. Acta Neuropathol 137:175–177. 10.1007/s00401-018-1935-7 [PubMed: 30446821]

23. Wen PY, Stein A, van den Bent M, De Greve J, Wick A, de Vos F et al. (2021) Dabrafenib plus trametinib in patients with BRAF(V600E)-mutant low-grade and high-grade glioma (ROAR): a multicentre, open-label, single-arm, phase 2, basket trial. Lancet Oncol. 10.1016/S1470-2045(21)00578-7

24. Wu Z, Abdullaev Z, Pratt D, Chung HJ, Skarshaug S, Zgonc V et al. (2021) Impact of the methylation classifier and ancillary methods on CNS tumor diagnostics. Neuro Oncol. 10.1093/neuonc/noab227

25. Yamasaki K, Nakano Y, Nobusawa S, Okuhiro Y, Fukushima H, Inoue T et al. (2020) Spinal cord astroblastoma with an EWSR1-BEND2 fusion classified as a high-grade neuroepithelial tumour with MN1 alteration. Neuropathol Appl Neurobiol 46:190–193. 10.1111/nan.12593 [PubMed: 31863478]

26. Zhou W, Laird PW, Shen H (2017) Comprehensive characterization, annotation and innovative use of Infinium DNA methylation BeadChip probes. Nucleic Acids Res 45:e22. 10.1093/nar/gkw967 [PubMed: 27924034]

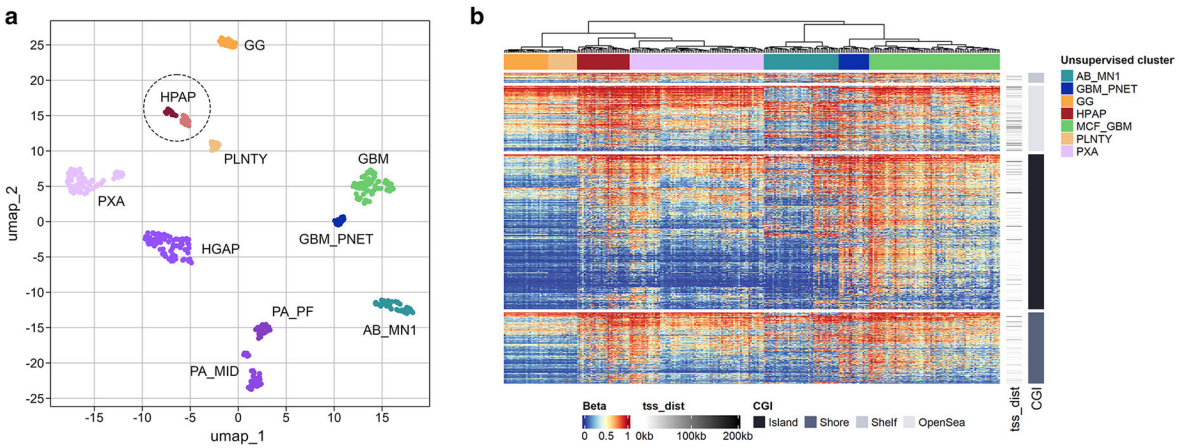

Fig. 1.

UMAP embedding of DNA methylation array data for select tumor types (**a**). Samples from this proposed group (HPAP, *n* = 31) embedded among select groups of CNS tumors enriched for *RB1* mutations (GBM_PNET, *n* = 19), *NF1* mutations (HGAP, *n* = 87; PA_PF, *n* = 28; PA_MID, *n* = 41), and *TP53* mutations (GBM, *n* = 77), as well as tumor types with similar histologic features (PXA, *n* = 79; AB_MN1, *n* = 46; PLNTY, *n* = 17). Two subtypes of HPAP, A and B, are readily distinguished. Hierarchical clustering of samples using the most variable probes and visualized across functionally important genomic regions (**b**). *AB_MN1* astroblastoma with *MN1*-alteration; *GBM* glioblastoma (or MCF_GBM methylation class family is comprised of the v11 methylation classes GBM_MES GBM_RTK1 and GBM_RTK2); *GBM_PNET* glioblastoma with primitive neuroectodermal features; *GG* ganglioglioma; *PLNTY* polymorphous low-grade neuroepithelial tumor of the young; *HGAP* high-grade astrocytoma with piloid features; *HPAP* high-grade glioma with pleomorphic and pseudopapillary features; *PA_MID* pilocytic astrocytoma midline; *PA_PF* pilocytic astrocytoma posterior fossa; *CGI* CpG island; *tss_distance* distance to the transcriptional start site

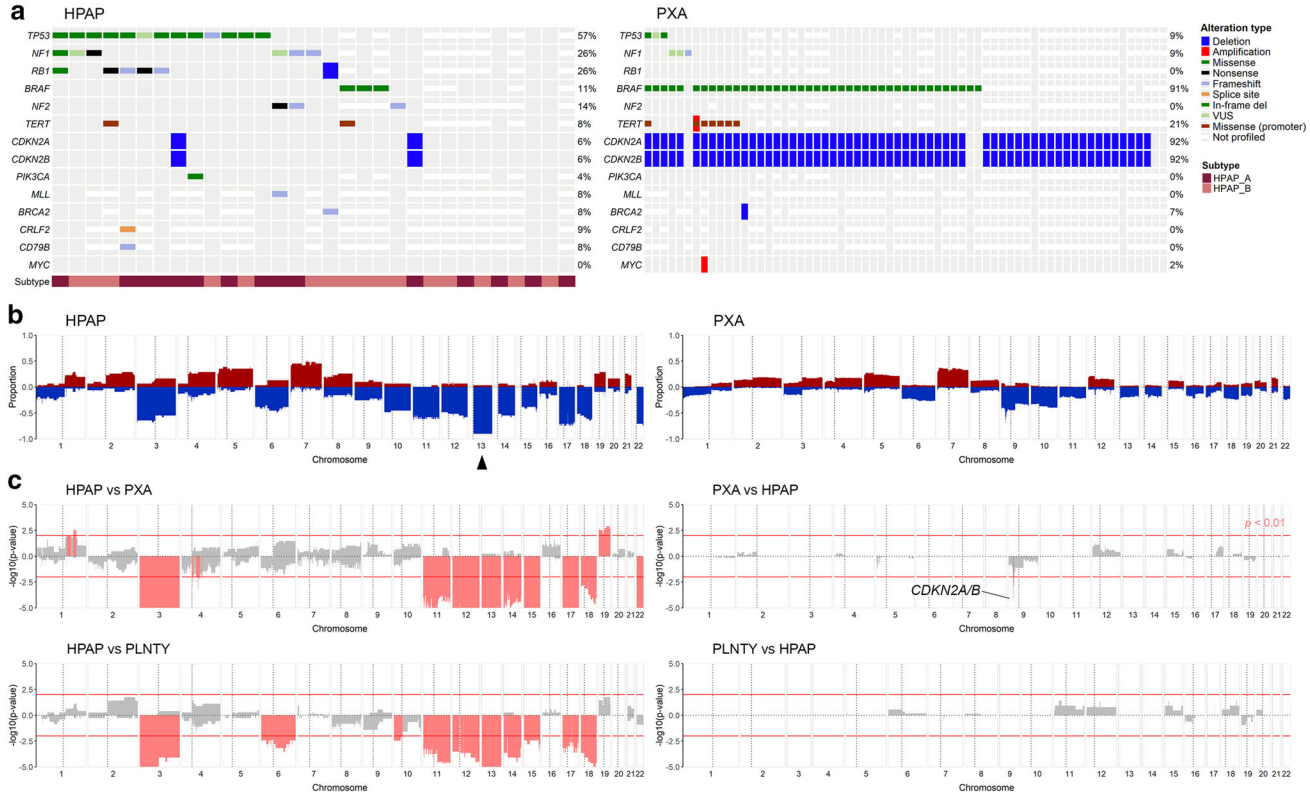

Fig. 2.

Recurrent genetic alterations in HPAP compared to PXA (**a**). Alteration frequencies shown to the right of each oncoplot represent the proportion of alterations among those tumors that were sequenced/profiled for that gene. Genome-wide copy number plots generated from methylation data for HPAP (left) and PXA (right) demonstrating enrichment for monosomy 13 in HPAP (arrowhead) (**b**). Genome-wide plot of the results of proportion tests for binned copy number regions in HPAP vs. PXA (**c**); regions with a statistically significant difference in the frequency of copy number alterations are highlighted in light red (HPAP vs. PXA, top; HPAP vs. PLTNY, bottom). Abbreviation: VUS, variant of unknown significance

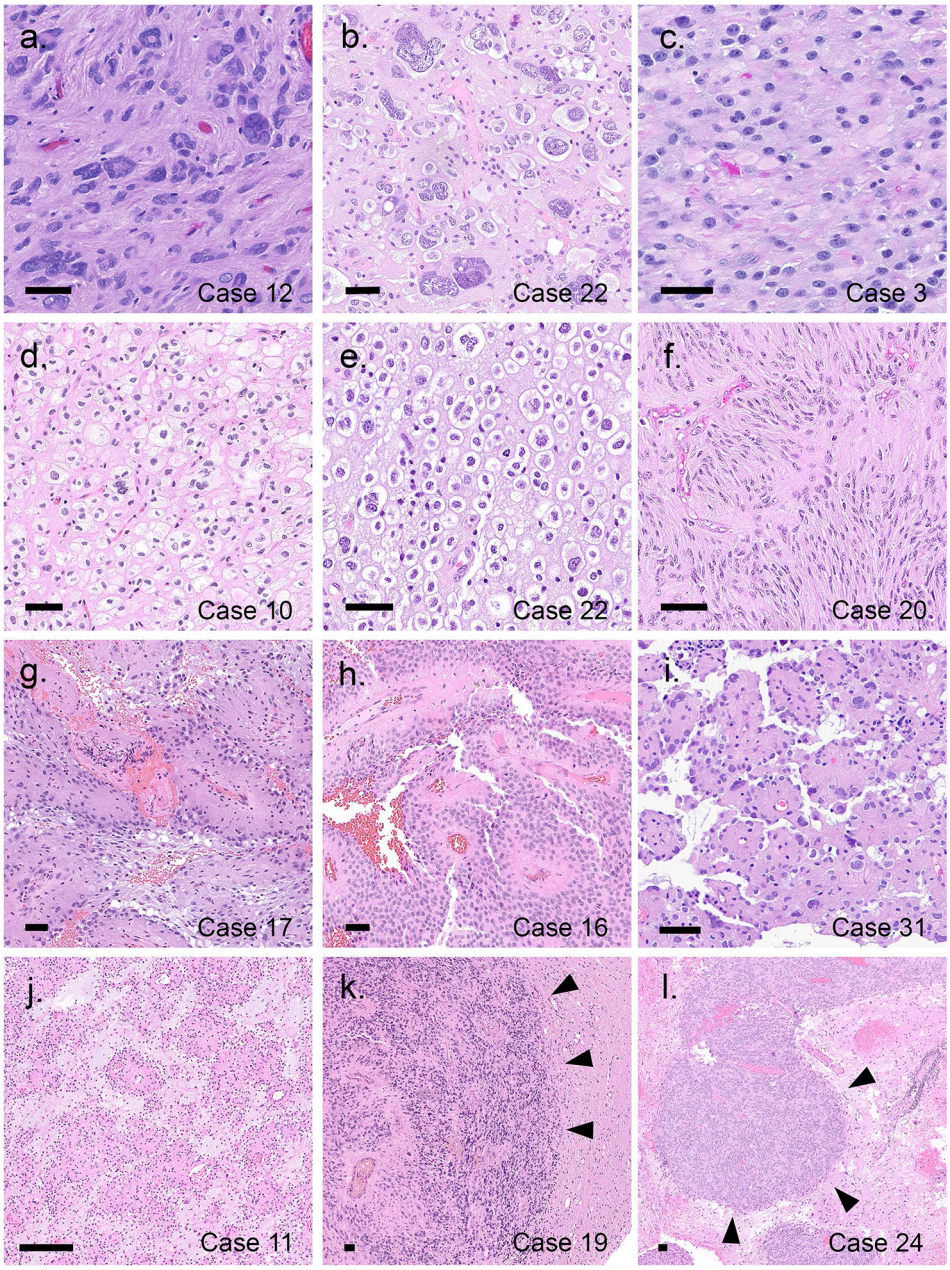

Fig. 3.

Spectrum of histologic patterns and morphology seen in this ► group. H&E-stained sections demonstrating markedly pleomorphic tumor nuclei and giant cell morphology (**a, b**) and an occasional monomorphic appearance with eosinophilic, gemistocytic-like cytoplasm (**c**). Other features included perinuclear clearing in tumor cells, similar to PLNTY (**d, e**) and an ependymoma-like perivascular arrangement of tumor cells (**f**). Pseudopapillary structures resembled astroblastoma in many cases (**g–j**). Tumors showed a predominantly non-infiltrative pattern of growth with identifiable borders (arrowheads) in many cases (**k, l**). Scale bars = 50 μm

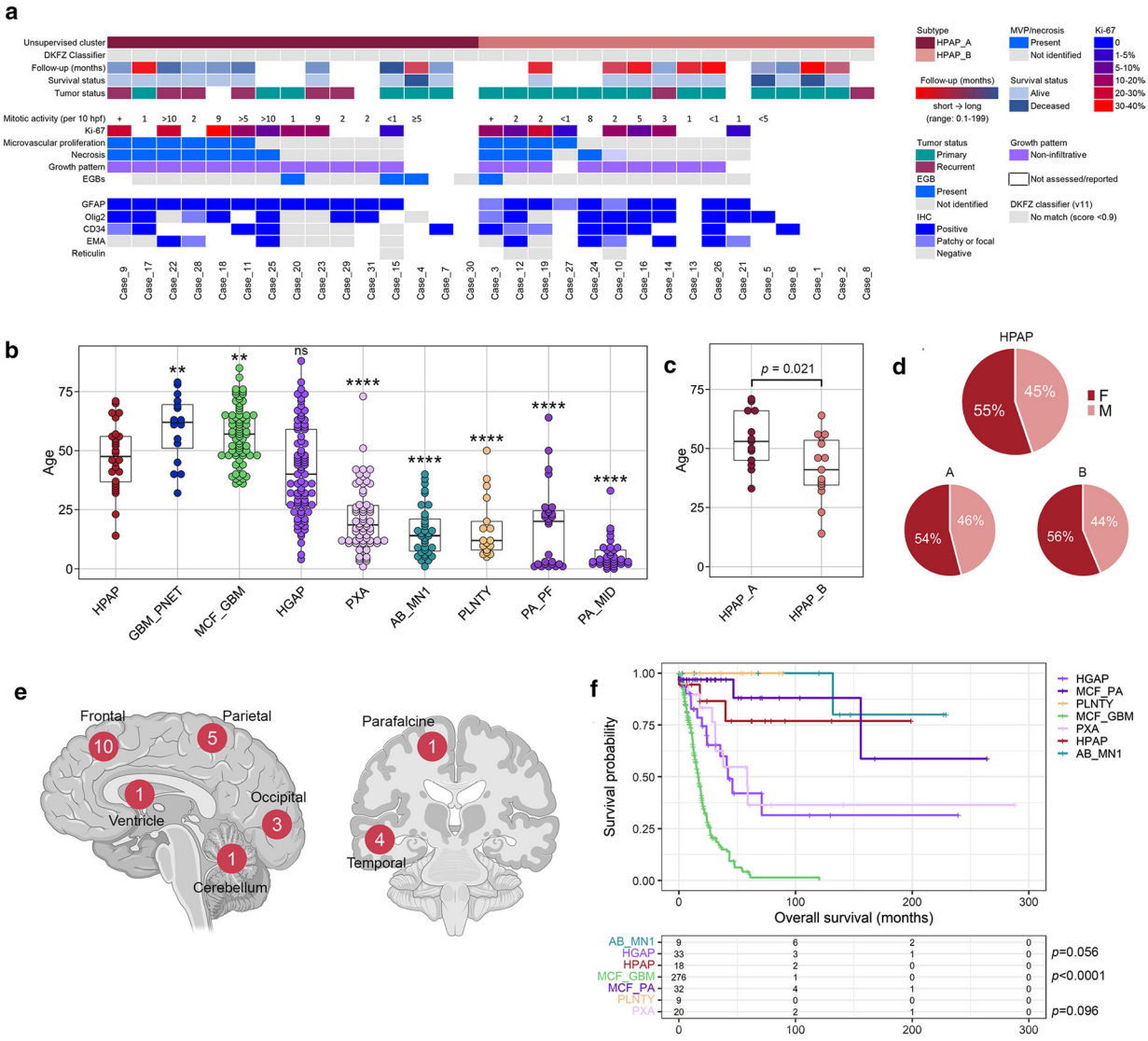

Fig. 4.

Clinicopathologic features. Oncoprint illustrating the frequency of various histologic and immunophenotypic features across evaluable samples (**a**); the corresponding subtype determined by dimensionality reduction (UMAP) and results of the DKFZ machine learning classifier (v11) are annotated. The age distribution across the tumor types included in this study (**b**); significance levels (asterisks) are results from comparison with HPAP. Box plot of age comparing the two subtypes of HPAP (**c**). Pie charts showing the distribution of biologic sex among HPAP and its subtypes (**d**). Illustration of the neuroanatomic distribution (**e**). Kaplan–Meier curves demonstrating differences in overall survival among tumor types for which data was available (**f**); the risk table shows the sample sizes in each group and the *p* value for select comparisons from the log-rank test with HPAP. Abbreviations: EGB, eosinophilic granular bodies; GFAP, glial fibrillary acidic protein; EMA, epithelial membrane antigen; MVP, microvascular proliferation; ns = $p > 0.05$, *$p \leq 0.05$, **$p \leq 0.01$, ***$p \leq 0.001$, ****$p \leq 0.0001$

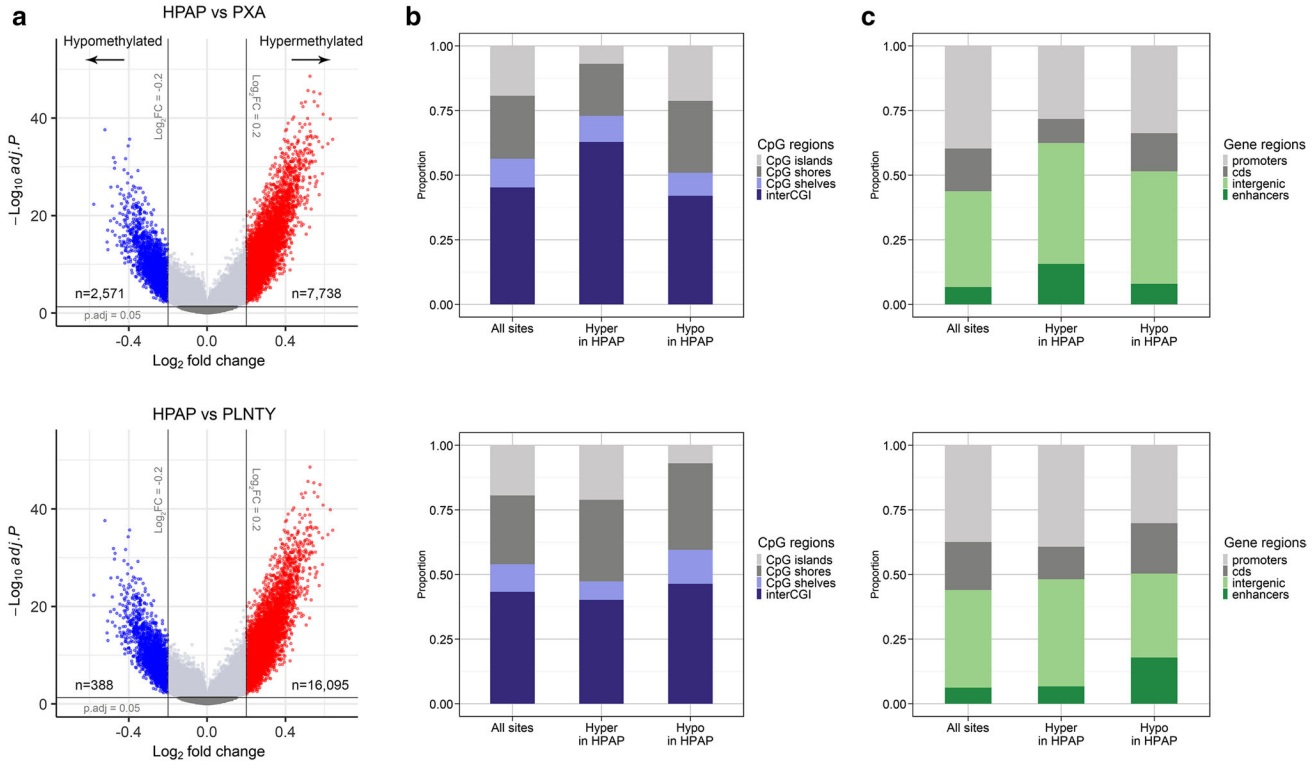

Fig. 5.

Differential methylation analysis. Volcano plots comparing differentially methylated probes between HPAP and PXA (top) and PLNTY (bottom) (**a**). The distribution of differentially methylated probes across CpG (**b**) and gene regions (**c**) for HPAP vs PXA (top) and HPAP vs PLNTY (bottom)